Supplementary Information

(1) Establishing the association of the 31 GeV photon with GRB 090510

The highest energy event detected with the LAT at a location similar to that of GRB 090510 has a reconstructed energy of ~ 31 GeV and was observed ~ 0.829 s after the GBM trigger. This event is important for the derivation of stringent limits on possible Lorentz invariance violation, expected in some quantum-gravity models that invoke an energy-dependent speed of light (see also section 6). It also plays an important role in setting strict lower limits on the bulk Lorentz factor of the emitting region (see section 3) and in the identification of a high-energy spectral component (see subsection 4 A). To proceed in all these derivations, we, therefore, need to evaluate the probability of this event being a photon coming from GRB 090510 and give a precise estimate of a best energy confidence interval.

The high-energy particle crossed the LAT without firing any Anti-Coincidence Detector tiles and the first tracker silicon strip detectors were left with no signal. These are characteristics of a neutral particle. A compact and symmetric cluster was produced in the calorimeter, with its main axis nicely aligned with the reconstructed track. This signature of an electromagnetic shower confirms the particle as a photon.

The angular separation of the reconstructed direction of the photon to the best localization found with the Swift-UVOT (R.A. $= 333.55208$, Dec. $= -26.58311$ with a 90% confidence error radius of 1.5 arcsecond), is found to be 5.8 arcmin, which is perfectly consistent with the point spread function of the LAT instrument at this energy (95% PSF at ~ 30 GeV is ~ 16 arcmin for this type of LAT events).

Another important line of evidence in favor of the event association with GRB 090510 is the fact that it is detected in temporal coincidence with the lower energy emission from this burst. To calculate the chance probability that this photon is not physically associated with GRB 090510 and is instead a background event, we used a background-estimation method described in[SI1] that has an accuracy of $\sim 15-20\%$. The expected number of background events was estimated to be 9×10^{-6}, and the associated probability of detecting at least one event when expecting that number of background events was 9×10^{-6} or $4.4\,\sigma$ (for a two-sided Gaussian distribution).

However, the 31 GeV event only barely missed the "diffuse" event Classification[SI2]; as a result its associated significance should be higher than $4.4\,\sigma$, since a diffuse-class event

Instrument	T_{90} (s)	T_{50} (s)
GBM/NaI 3	0.6	0.2
GBM/NaI 6	9.0	0.3
GBM/NaI 7	1.5	0.2
GBM/NaIs 3, 6 & 7	2.1	0.2
Swift/BAT	4.0	0.7
INTEGRAL-SPI	2.5	0.1
Suzaku-WAM	5.8	0.5

Table 1. Durations of GRB 090510 detected with different instruments.

can be identified as a photon with a considerably greater certainty. Therefore, it would be worthwhile to repeat the above calculation using the expected number of diffuse-class events instead and use the result as an upper limit on the 31 GeV photon significance. The actual significance should be closer to this upper limit. We find that the expected number of diffuse-class background events is 1.7×10^{-8} and an associated probability 1.7×10^{-8} or $5.6\,\sigma$. Therefore, the significance of the 31 GeV photon is between $4.4\,\sigma$ and $5.6\,\sigma$, with a most likely value close to the upper bound, i.e. a significance of above $5\,\sigma$.

Having characterized this event as a photon and established its association with GRB 090510 with a high degree of confidence, we find the best estimate for its energy to be 30.53 GeV with 1-σ and 2-σ confidence intervals of 27.97 – 36.32 GeV and 25.86 - 42.94 GeV, respectively.

(2) GRB 090510 Duration and Lag Analyses

A. Duration

We have applied the technique described in[SI3] to determine the T_{90} and T_{50} durations * of GRB 090510 using data from multiple instruments (see Table 1). The wide range in T_{90} durations exhibited in Table 1 is best illustrated in Figure 1, where we have plotted the cumulative counts for two detectors (GBM/NaI6 and Swift/BAT) integrated over the energy range 50 – 300 keV. Ideally, the selection of the 0% and the 100% levels in the plot (which appear as plateaus designating the onset and the end of the burst data accumulation) is unambiguous; however, when large background variations exist, the plateau selection is non-unique as one can see in the upper panel of Figure 1. The most

*The definition of T_{90} (T_{50}) is the time between accumulating 5% and 95% (25% and 75%) of the counts associated with the GRB.

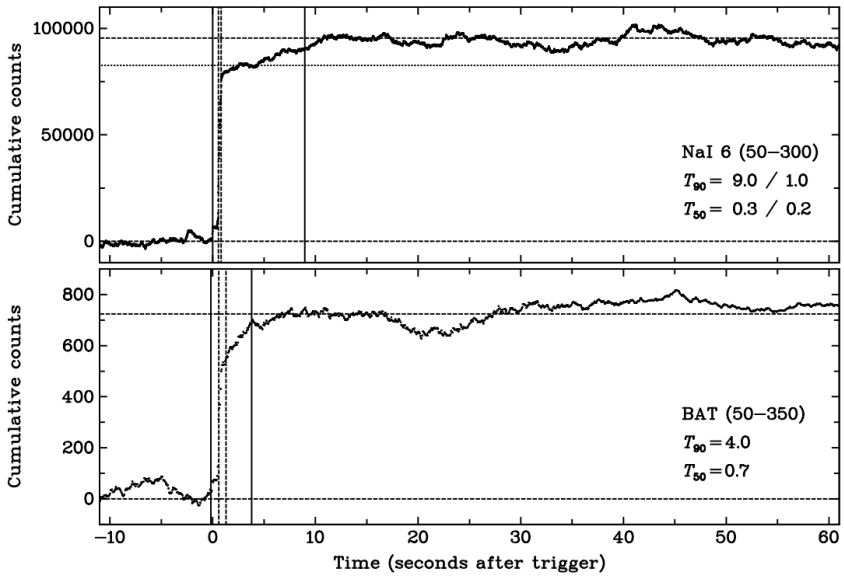

Figure 1. GRB 090510 T_{90} and T_{50} estimates using GBM/NaI 6 and Swift/BAT.

conservative selection (dashed line) provides $T_{90} = 9.0$ s, while alternative selections give lower values (down to 1.1 s for the dotted line). The lower panel, however, allows for one setting of the 100% level, which provides $T_{90} = 4.0$ s. Similar plots have been obtained for other GBM detectors, the INTEGRAL-SPI and the Suzaku-WAM. Our results are summarized in Table 1, which also shows the narrow range of T_{50}'s, compared to the T_{90} durations for each instrument. The latter are very sensitive to 5% background variations, while the former are more robust.

B. Spectral Lags

Spectral evolution is an established characteristic in GRBs, namely the trend for their high-energy photons to arrive before the lower-energy ones ("hard-to-soft" evolution). This trend, however, has been observed mainly at long GRBs and at lower energies typically $\lesssim$ 1 MeV. In contrast, short GRBs typically exhibit zero lags at these energy ranges.[SI4] To estimate the spectral lags for the light curves of GRB 090510 in different energy bands we have used here two independent methods: the cross-correlation function (CCF) method, and the method described in.[SI5]

1. Cross Correlation Function

We added the GBM Time Tagged Event light curves with 100 ms time resolution at

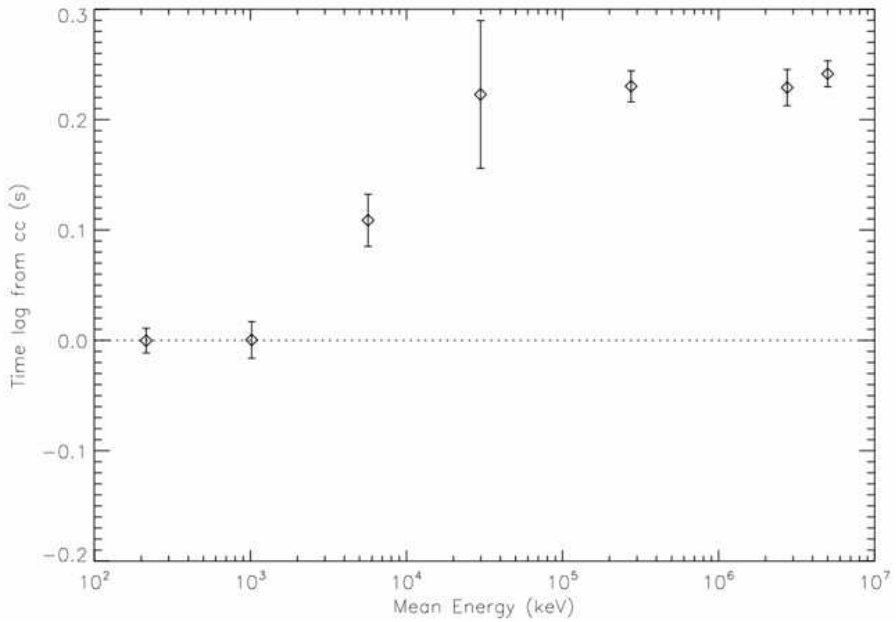

Figure 2. Time lags versus energy for GRB 090510.

8 logarithmic energy bins of the 2 brightest NaI detectors (6 & 7). The lower energy boundaries are 8, 20, 41, 70, 140, 270, 520, and 980 keV. Similarly, both the BGO light curves are added and divided into 8 energy bins with the lower energy boundaries at 0.11, 0.25, 0.55, 1.38, 3.33, 7.77, 19.2, and 45.5 MeV. For the LAT, we used all photons >100 MeV, which we subdivided into 3 light curves with lower energy boundaries of 0.1, 1, and 10 GeV. The mean energy for each light curve was taken as the arithmetic mean of the energy boundaries of a bin.

The peak of each cross-correlation plot is estimated by fitting a parabola to the 3 highest points. The computation of the error on the delays is based on the uncertainties of the fit parameters. The errors on the CCFs are estimated using Bartlett's formula[SI6] and are propagated to the errors of the peak position. We used three resolutions (10, 25 and 100 ms) and verified that our results did not change significantly.

We performed CCFs between the GBM/NaI and the GBM/BGO detectors as well as between the GBM and the LAT. All lags were estimated with respect to the summed lowest energy (8 – 40 keV) light curves of the NaI detectors; the results are shown on Figure 2. The first 4 points on the Figure are the spectral lags of the BGO light curves

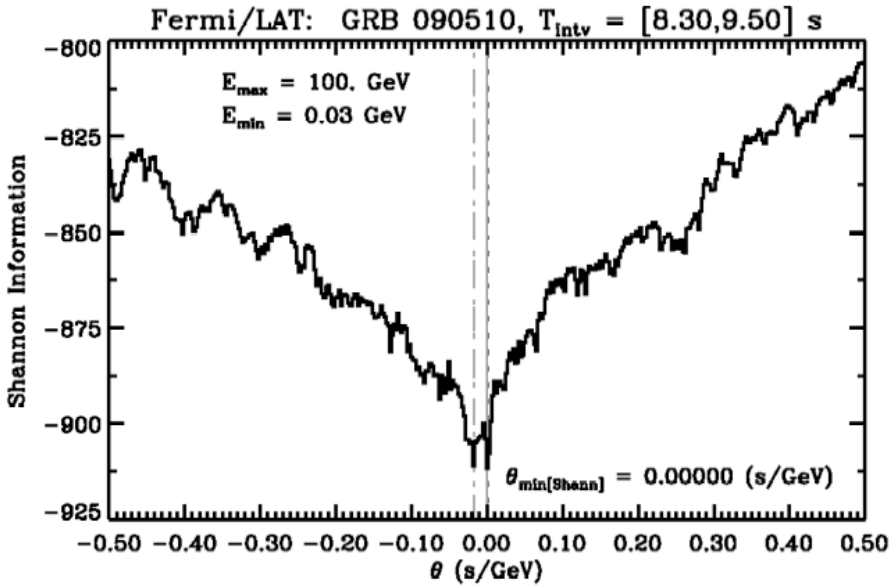

Figure 3. Shannon Information versus trial values of θ for the interval $T - T_{0,*} = 0.50 - 1.45$ s. The best value of θ is annotated, and shown as a vertical solid line. The two dashed vertical lines left and right of the best value represent the θ values which are $0.01\times$ less probable than the best θ value, *for the given data set*. Thus the contained interval between the two dashed lines is an approximate error region, but *does not reflect statistical uncertainties*.

with respect to the NaI base band-width and the last 3 points are the lags of the LAT data.

We find that below 1 MeV the spectral lags are negligible. Their values then progressively increase until about 30 MeV, and remain constant thereafter; the average lag between 40 and 1 MeV is 248 ± 34 ms. These results have been independently confirmed using CCF and the[SI5] method described below.

2. LAT only spectral lag analysis

Using the spectral lag procedure described in[SI5] we measured an upper limit on the spectral lag within the LAT energy range using photons with energies in the range $\sim$ 30 MeV – 30 GeV, in the interval $T - T_0 \simeq 0.50 - 1.45$ s, the burst interval with the most intense emission. Variation of stop times for this interval (± 0.25 s), and of energy upper limits (1, 3 & 100 GeV) did not significantly change the results described here.

The lag analysis yields a "best value" for the parameter θ, in s/GeV. This parameter is an effective lag measurement. The native LAT photon data are utilized, *unbinned*

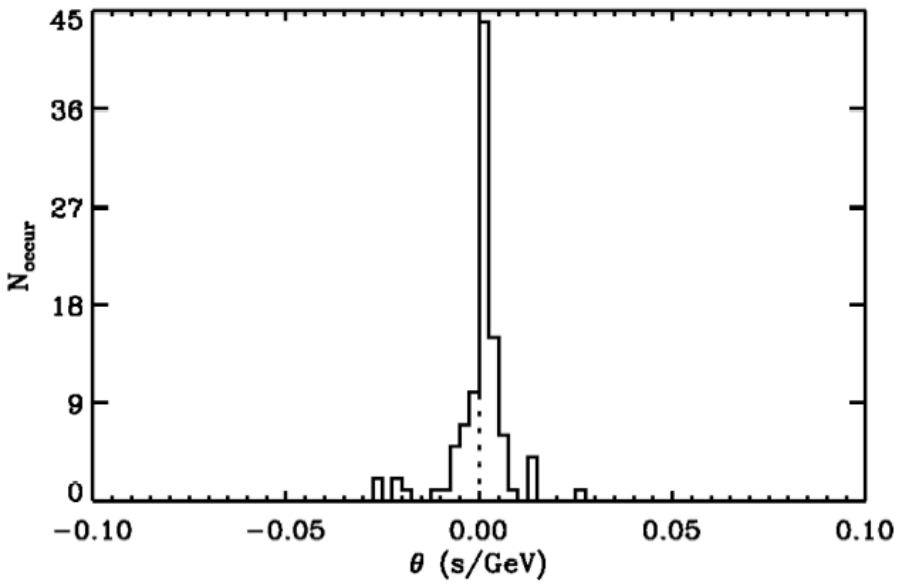

Figure 4. For the interval analyzed in Figure 3, to gauge uncertainty due to statistical variations we generated 100 realizations with the photon times randomized. $\theta_{\rm min}$ for these 100 realizations is within the range ± 0.03 s/GeV.

in time and energy. The procedure reassigns the times of the photons in several trial transformations, according to the photon energies. The trial, which results in the minimal value of a cost function, yields the "best value" for an energy-dependent lag. We employ transformations where the trial times are related to the energies linearly,

$$t'_{\rm i} = t^{\rm obs} - \theta E^{\rm obs}_{\rm i}. \tag{1}$$

The cost function is Shannon Information (eq. 11 of[SI5]), most frequently the cost function which yields the smallest statistical errors in simulations,

$$I({\rm Shannon}) = \sum_i p_{\rm i} \log(p_{\rm i}), \tag{2}$$

where the $p_{\rm i}$ are (one-dimensional) inverse densities: single counts (photons) in the inverse of time intervals. This particular cost function in another guise (modulo a minus sign) is *entropy*, and the difference of two values of θ is a *relative* probability that one value is more likely *for the given data set*.

Figure 3 illustrates the run of this cost function for trial values of θ, for the interval

$T - T_{0,*} = 0.50 - 1.45$ s and an energy upper limit of 100 GeV, with $\theta_{\rm min} = 0^{+2}_{-18}$ ms. Similar results were obtained when the time interval was varied slightly and the upper energy limit lowered to 3 GeV and 1 GeV. The error bars on $\theta_{\rm min}$ represent uncertainties inherent in the actual data, and thus do not include the statistical contribution which would result from measuring the burst several times, or with several identical detectors.

To estimate confidences that include statistical uncertainties, we performed 100 realizations of the LAT data with the energies randomly reassigned to the original times. The reassignment should destroy any correlation with energy and a histogram of $\theta_{\rm min}$ for the 100 realizations should be centered near zero. The results are shown in Figure 4. For these 100 realizations $\theta_{\rm min}$ lies within the range ± 0.03 s/GeV. Thus, at the 99% confidence level, the absolute value of the energy-dependent lag for the intense portion of GRB 090510 is <30 ms/GeV. The 90% confidence limit is about ± 10 ms/GeV.

(3) Details of the spectral analysis of the prompt GRB Spectrum

A. Observational Analysis

1. Data analysis

a. GBM data

GRB 090510 was very bright; as a consequence it was observed by many GBM detectors. For this analysis, we used the brightest detectors, including NaI detectors n3, n6, n7, n8 and n9 (8 keV − 1 MeV), and the two BGO detectors, b0 and b1 (200 keV − 40 MeV). Usually, the BGO detector in the source line of sight is more directly illuminated than the other BGO detector, which is blocked by the spacecraft and thus, unusable. In the case of GRB 090510, however, both BGO detectors were similarly illuminated and are therefore, used in the analysis. We used Time-Tagged Events (TTE) data with the overflow energy channels removed.

The background for each GBM detector was defined by fitting data before and after the burst with a polynomial function and then, this function was extrapolated to estimate the background during the burst. We custom-made detector response files for the various GBM detectors using the well-determined Swift/UVOT location.

b. LAT data

Energy-dependent selections of the LAT data were made based on the 95% PSF of the LAT detector. Again, we used the Swift/UVOT position with the error localization added in quadrature. For this analysis, the transient sources were analyzed with the

current standard LAT cuts, known as P6_v3_TRANSIENT. The background during the burst was computed by averaging the LAT background over several orbits of the spacecraft with the same position and the same pointing.

c. Analysis method

Joint analysis of the GBM and LAT prompt emission was performed with the *rmfit* software developed by the GBM team. The fits were then evaluated with a likelihood-based statistical technique (Castor statistic; C-stat).

2. Analysis of the systematics of the extra spectral component

We estimate here the systematic error on the significance of the extra spectral component. We consider two major sources for this systematic error: 1) the uncertainties of the effective area for both the LAT and GBM, and 2) the uncertainties of the background model of the GBM. We examined the spectral parameters and the significance of the extra component by changing in turn the effective area of the LAT and GBM by 10%.

Two methods were used for this adjustment of the effective area: with and without energy dependence. For the former method, we adjust the effective area only below 1 GeV and above 500 keV for the LAT and GBM, respectively, where the variation of the effective area becomes large. Using our custom detector responses with adjusted effective area, we then performed time-resolved spectral analysis in the same manner as the time-averaged spectral analysis, and compared the likelihood ratio of a single Band function with a Band function plus a power-law model. We found no large difference in the values of the spectral parameters; even with 10 % uncertainty in the effective area, the detection significance of the extra component remained larger than 5 σ as is shown in Figure 5.

We also investigated the effect of the uncertainties of the GBM background model. As described above and in Abdo et al. (2009), the background spectra of the GBM detectors are obtained by energy-dependent polynomial fitting of the light curve of each detector. The polynomial order is selected to minimize χ^2 for each energy channel and this selection could be the source of the systematic uncertainties. To investigate this effect, we generated the GBM background using different orders of polynomial functions and performed spectral analysis applying the respective background spectra. We found no background dependence on the polynomial order, because the background profile around the burst time interval was quite stable. We can thus conclude that the extra component found by our time-resolved analysis is not due to systematic effects caused by the uncertainties of the effective area and of the background model of the GBM.

We also checked the validity of our estimated significance for the extra component.

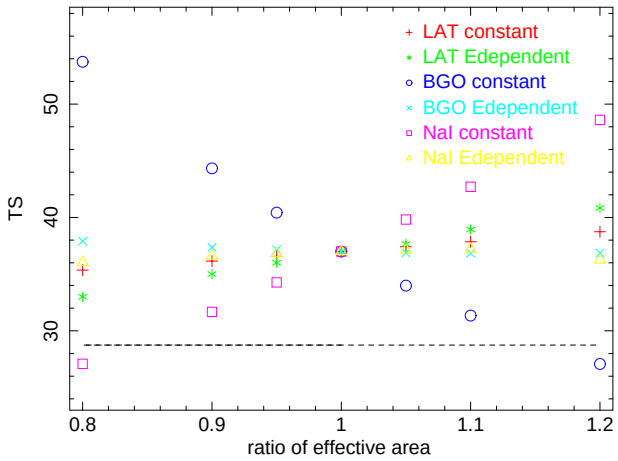

Figure 5. Relation between adjusted effective area and significance (TS) between single Band function and the Band function plus extra power-law component. Various patterns of adjustment of the effective area are shown in the figure: Red crosses and green asterisks show the adjustment of the LAT effective area without and with energy dependence, blue circles and cyan crosses for the GBM/BGO detectors, magenta squares and yellow triangles for the GBM/NaI detectors, respectively. The 5 σ significance limit is indicated by horizontal dashed-line.

This estimate was performed by assuming that the likelihood ratio between a single Band function and a Band plus power-law model follows the χ^2 distribution with 2 degrees of freedom. To test this assumption, we generated 6000 simulated spectra using the spectral parameters obtained by a single Band function and compared the likelihood ratio between the two models for our simulated spectra. We found that the obtained likelihood ratio follows the χ^2 distribution with 2 degrees of freedom, thus validating our significance estimate.

3. Are the high and low energy spectral components correlated?

We performed a simple but robust analysis aimed to quantify the correlation between the two spectral components identified with the low and high energy emission during the prompt phase of GRB 090510. Besides the first peak of the GBM light curve, where no significant emission has been detected in the LAT light curve, the subsequent GBM pulses appear correlated with the LAT ones in the time window between $0.6-0.8$ s after T_0. The low energy component is dominant in the GBM/BGO band, while the high-energy one dominates at energies above 20 MeV, in the LAT detector data.

To minimize the overlap between the GBM and LAT light curves we consider only

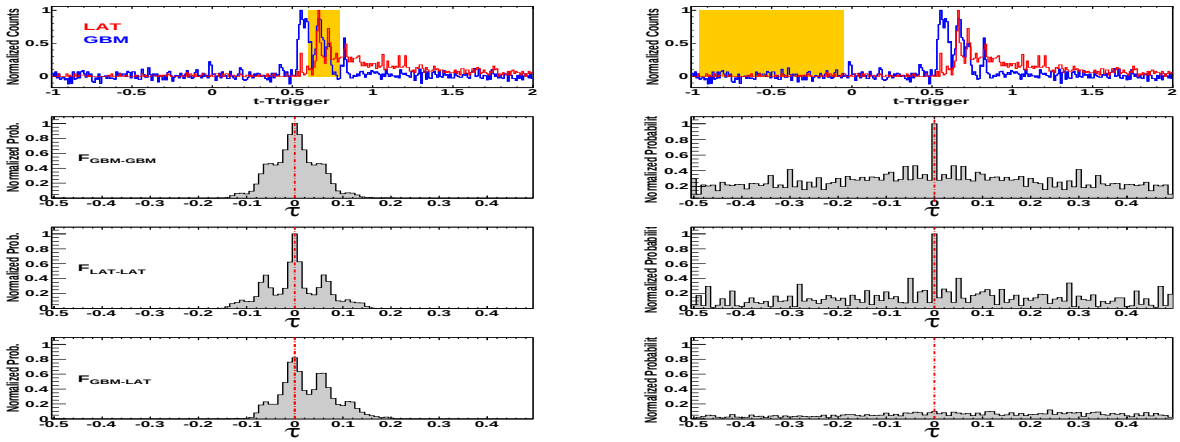

Figure 6. Left panels: Top panel: BGO (blue) and LAT (red) light curve, normalized to unity. The shared area is the portion of the light curve where an extra component is clearly visible in the spectra, and highlights the region of the light curve we have used for this analysis. The second panel displays $F_{\rm GBM-GBM}$ which has been normalized to one. The function $F_{\rm LAT-LAT}$ is displayed in the third panel, also normalized, while the last panel shows the correlation between LAT and GBM ($F_{\rm GBM-LAT}$). **Right panels**: same as *left panels*, but the analysis has been applied to background, in the region highlighted with an orange box.

the events in the GBM detector between 250 keV and 3 MeV (hereafter GBM), and we use the "full LAT" light curve (hereafter simply LAT) to get enough statistic. The two light curves (blue GBM, red LAT) are displayed in the top left panel of Fig. 6, where the shaded orange area highlights the region selected for this study.

The first step of our analysis is to normalize both light curves to unity, to avoid effects due to the relative magnitude of the signal. Then we compute the quantity:

$$F_{\rm GBM-LAT}(\tau) = \frac{2\sum_{i=i_1}^{i_2}\left[({\rm GBM}(t_i)\cdot{\rm LAT}(t_i+\tau)\right]^2}{F_{\rm GBM-GBM}(0)+F_{\rm LAT-LAT}(0)}, \quad (3)$$

where i_1 is the time where $t = T_0 + 0.6$ s, i_2 is the time bin at which $t = T_0 + 0.8$ s and i is the $i^{\rm th}$ bin. We refer to this function as the "correlation" function for simplicity, even if, formally, it is not a convolution integral.

We then compute the square of the product between the GBM normalized light curve and the "shifted by tau" normalized LAT light curve. This product has a maximum when the peaks of the two shifted light curves coincide. To exclude the possible contribution

from regions outside the time window under study, we also impose that $i + \tau < i_1$ and $i + \tau > i_2$.

To normalize our method, we first compute the "correlation" between the GBM light curve with itself ($F_{\rm GBM-GBM}$), and the LAT light curve with itself ($F_{\rm LAT-LAT}$). We obviously expect these curves to have a maximal correlation at $\tau = 0$, thus we normalize the functions accordingly, setting $F_{\rm GBM-GBM}$=1 and $F_{\rm LAT-LAT} = 1$ (100% correlation at zero). The scaling factors used are $F_{\rm GBM-GBM}(0)$ and $F_{\rm LAT-LAT}(0)$, respectively. The resulting correlation curves are shown in the second and third left panels of Fig. 6.

Finally, we computed the correlation function between the GBM and LAT light curves, normalizing the histogram to the average between the scaling factor of the previous two histograms, namely equation 3. The results are shown in the bottom left panel of Fig. 6.

The function $F_{\rm GBM-LAT}(\tau)$ has a maximum of 0.8 at τ=0, and a second maximum of 0.6 at $\tau \approx 0.06$, when, in practice, the second peak of the LAT light curve overlaps with the third peak of the GBM one. Our analysis thus shows that the two curves have the best correlation when no shift of time is applied, supporting the hypotheses that the two spectral components originate from the same physical region.

To estimate the uncertainties of our method, we have performed an identical analysis selecting a region of the light curve before the time of the trigger between $(-0.95, -0.05)$ s, consisting entirely of uncorrelated background in the two different detectors. We repeat the steps described above on the region highlighted by the shaded area in the top right panel of Fig 6. The results, displayed in Fig. 6, set a value of 0.1 (10%) for the uncertainty on the determination of the correlation with this technique.

B. Theoretical Implications of the High-Energy Spectra

The emergence of a distinct high-energy spectral component in the prompt-phase spectrum of GRB 090510 tests emission models of GRBs, in particular, whether the high-energy γ rays have leptonic or hadronic origin. In either type of model the dominant emission mechanism during the prompt phase is unclear. The keV – MeV radiation could be nonthermal synchrotron radiation, in which case an associated synchrotron self-Compton (SSC) spectral component is expected at GeV – TeV energies. The observed > 100 MeV γ rays could originate from hadronic processes, either through proton- or ion-synchrotron radiation in highly magnetized emission regions, or from secondary radiations induced by photohadronic proceses.

Nonthermal Synchrotron and SSC:

GRB outflows must be ultra-relativistic (see § 5). The internal photon energy density of the radiating region of GRB 090510 is given by

$$u'_\gamma \cong \frac{d_L^2(1+z)^2\Phi}{\Gamma^6 t_v^2 c^3} \cong 4.4\times10^6\,\frac{(\Phi/10^{-5}\ \mathrm{erg\ cm^{-2}s^{-1}})}{\Gamma_3^6\,(t_v/10\,\mathrm{ms})^2}\ \mathrm{erg\ cm^{-3}}\ , \tag{4}$$

where Φ is the observed energy flux whose variability timescale is t_v, d_L is the luminosity distance of a source at redshift z ($z = 0.903$ and $d_L = 1.8\times10^{28}$ cm for GRB 090510), $\Gamma = 10^3\Gamma_3$ is the outflow Lorentz factor, and $R \cong c\Gamma^2 t_v/(1+z)$ is assumed. The magnetic field, of comoving energy density $u'_B = (B')^2/8\pi$, can be expressed in term of u'_γ as

$$B' \equiv \sqrt{8\pi\psi u'_\gamma} \cong 10\frac{\sqrt{\psi(\Phi/10^{-5}\ \mathrm{erg\ cm^{-2}s^{-1}})}}{\Gamma_3^3\,(t_v/10\,\mathrm{ms})}\ \mathrm{kG}\ , \tag{5}$$

through a parameter $\psi \equiv u'_B/u'_\gamma$. The minimum apparent isotropic jet power

$$P_j = 4\pi R^2\beta c\Gamma^2(u'_B + u'_{par})\ , \tag{6}$$

where u'_{par} is the co-moving particle energy density. For GRB 090510, the apparent isotropic jet power from the magnetic field alone is $P_j^B \cong 4\times10^{52}\psi\Phi_{-5}$ erg s^{-1}. The corresponding particle power depends on the specific synchrotron/SSC model.

If the keV–MeV radiation in GRBs is nonthermal synchrotron emission radiated by nonthermal relativistic electrons, then the corresponding synchrotron self-Compton (SSC) emission may be detected at GeV – TeV energies. In the Thomson regime, whose criterion is $\epsilon_{\rm C}\epsilon_s \lesssim [\Gamma/(1+z)]^2$, the outflow Lorentz factor and magnetic field in a nonthermal synchrotron/SSC model are given by[SI7]

$$\Gamma \cong \frac{1}{\epsilon_s}\sqrt{\frac{\epsilon_{\rm C}}{ct_vB_{cr}}\sqrt{\frac{2L_s}{cy_{\rm C}}}}\ , \qquad B \cong \frac{(1+z)B_{cr}\epsilon_s^3}{\epsilon_{\rm C}^{3/2}}\sqrt{ct_vB_{cr}\sqrt{\frac{cy_{\rm C}}{2L_s}}}\ , \tag{7}$$

where the peak synchrotron (SSC) νF_ν flux f_{ϵ_s} ($f_{\epsilon_{\rm C}}$) is measured at peak dimensionless (in units of m_ec^2) photon energy ϵ_s ($\epsilon_{\rm C}$), $y_{\rm C} \equiv f_{\epsilon_{\rm C}}/f_{\epsilon_s}$ is the Compton y-parameter, and $B_{cr} = m_e^2c^3/e\hbar \cong 4.414\times10^{13}$ G is the critical magnetic field.

In addition, the derived value of Γ from eq. (7) must be larger than $\Gamma_{\rm min}$, derived from $\gamma\gamma$ opacity constraints. Provided the target photon spectrum is softer than +1 in νF_ν index, the minimum bulk Lorentz factor from $\gamma\gamma$ opacity arguments for a high-energy γ-ray photon with dimensionless energy ϵ_1 can be simply expressed as

$$\Gamma_{\rm min} \approx \Big[\frac{\sigma_{\rm T}d_L^2(1+z)^2 f_{\hat\epsilon}\epsilon_1}{6t_vm_ec^4}\Big]^{1/6}\ ,\ \ \hat\epsilon = \frac{2\Gamma^2}{(1+z)^2\epsilon_1}\ . \tag{8}$$

Lack of any evident hard SSC component during the early soft phase at $T_0 + 0.5$ s to $T_0 + 0.6$ s with the minimum Lorentz factor constraint is compatible with a synchrotron/SSC origin if the peak of the SSC component is $\gtrsim$ TeV energies, in which it is strongly attenuated by $\gamma\gamma$ processes. Interpreting the hard component as a self-Compton component challenges leptonic models when the $\gamma\gamma$ opacity constraint is included. Allowable synchrotron/SSC models in terms of apparent isotropic jet powers and the $\gamma\gamma$ opacity constraint restrict leptonic models of this sort to ~ 10 G $\lesssim B' \lesssim 10^5$ G and $10^3 \lesssim \Gamma \lesssim 3000$.

Hadronic Emission:

The very high bulk Lorentz factors and large radiation energy densities in GRB outflows make GRBs potential sources of ultra-high-energy cosmic rays (UHECRs).[SI8,SI9] The extra spectral component seen in GRB 090510 may be due to high-energy accelerated protons, for instance emission from photomeson-induced secondary particles or synchrotron emission from protons (e.g.[SI10,SI11,SI12,SI13,SI14,SI15]). Although the cascade processes initiated by $p + \gamma \rightarrow p/n + \pi^0/\pi^+$ are complicated, the resultant photon signatures of proton cascades appear mostly as synchrotron or Compton emissions from secondary electron-positron pairs produced via $\gamma + \gamma \rightarrow e^+ + e^-$. In such pair cascade processes the effective injection index of secondary pairs tends to be about[SI16] -2 so that the synchrotron radiation from secondary pairs yields a flat νF_ν spectrum, while the power-law index of the extra component in GRB 090510 is ~ -1.6. However, the Compton component from secondary pairs can harden the spectrum.[SI17]

In numerical approaches to this problem, physical processes taken into account include: 1) photon emission processes of synchrotron and Compton scattering for electrons/positrons, protons, pions, and muons; 2) synchrotron self-absorption of low-energy radiation; 3) $\gamma\gamma$ pair production; 4) photomeson production from protons and neutrons; 5) Bethe-Heitler pair production ($Z + \gamma \rightarrow Z + e^+ + e^-$); and 6) decays of pions and muons (for details of recent calculations, see Ref.[SI18]). The Compton radiation physics should be accurate throughout the Thomson and Klein-Nishina regimes.

An important feature in the spectral evolution of GRB 090510 is the delayed onset of the main $\gtrsim$ 100 MeV LAT emission relative to the main GBM emission, similar to the long-duration GRBs 080916C[SI19] and 080825C.[SI1] If the delayed onset is a common feature of long and short GRBs, then this might suggest a common emission mechanism.

Proton and ion synchrotron radiation from GRBs can provide an explanation for the delayed onset, but requires a highly magnetized emission region.[SI20] The scaling to a

short hard GRB depends primarily on the variability time and the magnetic field. The magnetic field estimate, eq. (5), for GRB 090510, gives

$$B'(100\ \mathrm{kG}) \cong \frac{2\Phi_{-5}}{\Gamma_3^3 t_v(10\ \mathrm{ms})} \quad , \tag{9}$$

for $\psi = 400$. The delayed onset in this model is due to the time for protons to accumulate and radiate synchrotron in the LAT band. The delay time can be expressed as

$$t_{dly}(\mathrm{s}) \cong 0.5\ \frac{(\phi/10)}{\Gamma_3 B_5'^2}\ \mathrm{s}\ . \tag{10}$$

This expression scales to give a delayed onset of a few tenths of a second for GRB 090510, taking $z = 0.9$ and $B' \approx 100$ – 200 kG. Thus, within the hadronic interpretation of the distinct high-energy spectral component in GRB 090510, even GRBs of the short-hard class appear capable of accelerating cosmic rays to ultra-high energies.

Photopion processes become important for protons of energy E_p when the photopion efficiency $f_{p\gamma}(E_p) = t'_{dyn}/t'_{p\gamma}(E_p)$ starts to approach unity. In a blast-wave framework the comoving dynamical time is $t'_{dyn} = R/\Gamma c$ and the comoving photopion loss timescale is $t'_{p\gamma} \approx cK_{p\gamma}\sigma_{p\gamma}\int_{\epsilon'_{thr}}^{\infty} d\epsilon' n'(\epsilon')$, where the photopion threshold photon energy is $\epsilon'_{thr} \cong 400\Gamma/\gamma_p$. Protons of energy $E_p^{br} \cong 400 m_p c^2\Gamma^2/[(1+z)\epsilon_{br}]$ preferentially interact with photons at the break energy ϵ_{br} in the GRB spectrum. The efficiency for photopion processes in GRB 090510 at $E_{br} \cong 2\times 10^{16}\Gamma_3^2/(\epsilon_{br}/10)$ eV can be expressed[SI8,SI21] as

$$f_{p\gamma}(E_p^{br}) = \frac{K_{p\gamma}\sigma_{p\gamma} d_L^2 f_{\epsilon_{pk}}}{\Gamma^4 m_e c^4 t_v \epsilon_{br}} \cong \frac{0.15(f_{\epsilon_{pk}}/10^{-5}\ \mathrm{erg\ cm^{-2}\ s^{-1}})}{\Gamma_3^4 t_v(0.01\ \mathrm{s})(\epsilon_{br}/10)}, \tag{11}$$

where $K_{p\gamma}\sigma_{p\gamma} \cong 70\mu$b. Protons with energy $E_p < E_p^{br}$ produce pions by primarily interacting with photons with $\epsilon > \epsilon_{br}$, and the efficiency $f_{p\gamma}(E_p) \propto E_p^{-1-\beta}$. Higher energy protons interact primarily with lower energy photons, so $f_{p\gamma}(E_p) \propto E_p^{-1-\alpha}$ when $E_p > E_p^{br}$ when $-1 \lesssim \alpha \lesssim -2$. Photohadronic processes could therefore make a high-energy γ-ray spectral component from multi-PeV protons in GRB 090510.

Such hadronic models also face challenges. They typically require a very large total energy, > 100 times larger than the observed energy in γ-rays. This may prove challenging for the progenitor of GRB 090510, whose apparent isotropic γ-ray energy release, $(1.08 \pm 0.06)\times 10^{53}$ erg, is at the top end of the short GRB distribution.

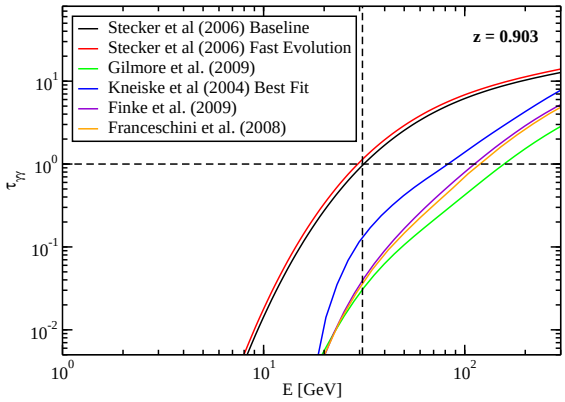

Figure 7. Model predictions of EBL absorption optical depth versus photon energy for GRB 090510.

(4). Possible Implications of Attenuation by Extragalactic Background Light

After the cosmic microwave background, the Extragalactic Background Light (EBL) extending from ultraviolet to infrared wavelengths is the most energetically intense background radiation. It is dominated by direct starlight in the optical/ultraviolet and stellar radiation that is reprocessed by dust in the infrared. The EBL is difficult to measure directly due to contamination by zodiacal and Galactic foreground light.[SI22]

EBL photons absorb gamma-rays by creating electron-positron pairs if the combined photon energies are above the pair creation threshold. Fig. 7 shows the absorption optical depth, $\tau_{\gamma\gamma}$, for various models of the EBL as a function of gamma-ray energy at the redshift $z = 0.903$ of GRB 090510. We have included curves for the two models of[SI23] as well as the fiducial model of,[SI24] the best fit model of,[SI25] the model by,[SI26] and "Model C" of.[SI27] Only the models of[SI23] are optically thick at the energy of the 31 GeV photon; all other models considered here give a transmission probability of $\exp(-\tau_{\gamma\gamma}) \gtrsim 85\%$. The baseline and fast evolution models of[SI23] give transmission probabilities of 37% and 30%, respectively. Although a higher energy photon was found from this burst (31 GeV) than for GRB 080916C (13 GeV;[SI19]), the latter burst was more constraining to the EBL due to its higher redshift of[SI28] $z = 4.35 \pm 0.15$.

Integrating the Band and Band+PL fits in individual time bins within the range 0.5–1.0 s (see main text Table 2), and summing over their contributions to the total fluence result in $E_{\rm iso} = (1.08 \pm 0.06) \times 10^{53}$ erg. When these are deabsorbed with the fast evolution model of[SI23] this increases $E_{\rm iso}$ by only $\sim 1\%$. Therefore, we conclude that the effect of EBL on the estimated value of $E_{\rm iso}$ within the observed energy range is negligible.

Time interval	$E_{\rm max}$ [GeV]	variability time [ms]		FWHM [ms]	
		NaI	BGO	NaI	BGO
0.6 s – 0.8 s	$3.43^{+0.34}_{-0.20}$	22.3 ± 3.3	19.7 ± 3.7	22 ± 2	14 ± 2
0.8 s – 0.9 s	$30.53^{+5.79}_{-2.56}$	17.7 ± 3.1	11.9 ± 2.6	16 ± 2	12 ± 2

Table 2. Variability time scales estimated from the variability index and the full width at half maximum (FWHM) of the pulse in NaI and BGO detectors at the two most relevant time intervals.

(5) Lower Limit ($\Gamma_{\rm min}$) on the Bulk Lorentz Factor Γ

High-energy γ-rays in the GRB relativistic outflow are subject to $\gamma\gamma \to e^+e^-$ absorption *insitu* by interacting with low-energy photons that are produced at the source. This process is most effective if the high-energy and low-energy (target) photons are produced in the same physical region. For a given set of observed properties, the $\gamma\gamma$ interaction rate and opacity in the emission region is significantly reduced if it moves at a highly relativistic speed corresponding to a bulk Lorentz factor $\Gamma \gg 1$, which allows for a larger emission radius and a smaller co-moving target photon density. Observation of a non-thermal GRB spectrum up to a very high energy $E_{\rm max}$ can be used to calculate the minimum bulk Lorentz factor, $\Gamma_{\rm min}$, of the relativistic GRB jet.[SI29,SI30,SI19]

Given a γ-ray flux variability time-scale t_v, an observed broadband photon spectrum $n(\epsilon)$ and the GRB redshift z, a general formula can be written for the optical depth of a high-energy photons of energy E to $\gamma\gamma \to e^+e^-$ pair production,[SI31,SI32]

$$\tau_{\gamma\gamma}(E) = \frac{3}{4}\frac{\sigma_T d_L^2}{t_v \Gamma}\frac{m_e^4 c^6}{E^2(1+z)^3}\int_{\frac{m_e^2c^4\Gamma}{E(1+z)}}^{\infty}\frac{d\epsilon'}{\epsilon'^2}\; n\left(\frac{\epsilon'\Gamma}{1+z}\right)\varphi\left[\frac{\epsilon' E(1+z)}{\Gamma}\right] \;, \qquad (12)$$

where d_L is the luminosity distance and σ_T is the Thomson cross-section. The function $\varphi[\epsilon' E(1+z)/\Gamma]$ is defined in Ref.[SI31] The derivation of $\Gamma_{\rm min}$ usually follows from the condition $\tau_{\gamma\gamma}(E_{\rm max}) = 1$, or equivalently $\tau_{\gamma\gamma}(E < E_{\rm max}) < 1$. If the target photon spectrum can be fitted with a Band function, $\Gamma_{\rm min}$ can be calculated analytically with a delta-function approximation for the $\gamma\gamma \to e^+e^-$ total cross-section as

$$\begin{aligned}\Gamma_{\rm min}(E_{\rm max}) \;&=\; \left[\frac{4d_L^2 A}{c^2 t_v}\frac{m_e^2c^4}{(1+z)^2 E_{\rm max}}g\sigma_T\right]^{\frac{1}{2-2\beta}}\left[\frac{(\alpha-\beta)E_{\rm pk}}{(2+\alpha)100\ {\rm keV}}\right]^{\frac{\alpha-\beta}{2-2\beta}} \\ &\quad\times\exp\left(\frac{\beta-\alpha}{2-2\beta}\right)\left[\frac{2m_e^2c^4}{E_{\rm max}(1+z)^2 100\ {\rm keV}}\right]^{\frac{\beta}{2-2\beta}} \;; \\ &\quad {\rm for}\;\; \Gamma_{\rm min} > \sqrt{\frac{(1+z)^2 E_{\rm max}E_{\rm pk}(\alpha-\beta)}{2m_e^2c^4(2+\alpha)}} \;, \end{aligned} \qquad (13)$$

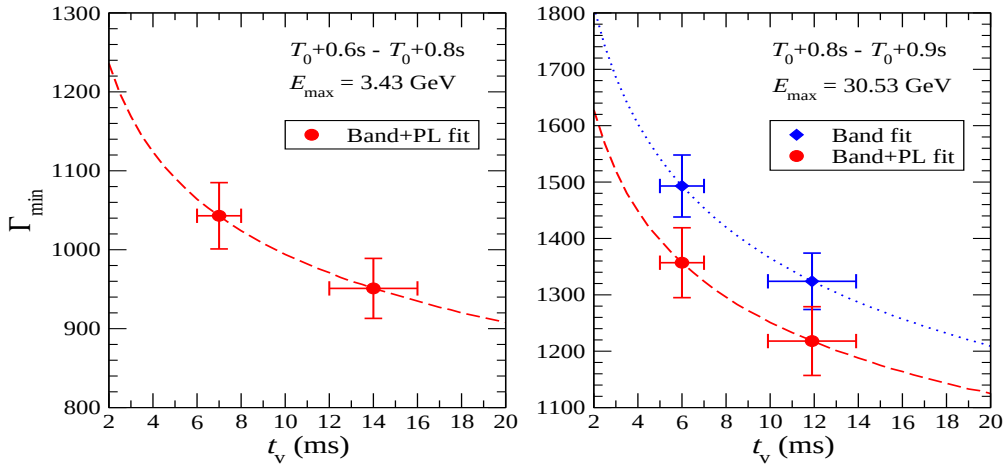

Figure 8. The minimum bulk Lorentz factor $\Gamma_{\rm min}$ of the GRB 090510 prompt mission region as a function of the γ-ray flux variability time-scale t_v, calculated using the time-averaged spectra in the time intervals 0.6 s – 0.8 s (*left panel*) and 0.8 s – 0.9 s (*right panel*) post-trigger. The highest-energy photon in each time-interval (see Table 2) is assumed to originate from the same physical region as the observed low-energy ($\sim$ MeV) photons in the same time interval (as suggested by the correlated variability at low and high energies; see subsection 3-A-5). The data points with error-bars correspond to the $\Gamma_{\rm min}$ calculated for the best-fit t_v = FWHM and FWHM/2 in the respective time intervals.

where A, $E_{\rm pk}$, α and β are the Band function parameters, and $g\sigma_T$ is the total $\gamma\gamma$ cross-section. The factor $g \approx 0.23$ and it depends on the target photon spectrum. Equation (13) agrees with the numerical solution to equation (12) for $\Gamma_{\rm min}$ to within a few percent.

The error on $\Gamma_{\rm min}$ can be calculated by varying individual parameters from a Band function fit, or a Band function and a power-law (Band+PL) fit within their 1-σ limits. For a given variability time, we use a $d \times d$ dimensional covariance matrix M constructed from the $(d-1) \times (d-1)$ dimensional covariance matrix for the Band fit or Band+PL fit parameters and the errors on the energy estimate of $E_{\rm max}$. The error on $\Gamma_{\rm min}$ is then $\delta\Gamma_{\rm min} = \sqrt{\tilde{D}MD}$, where D is a d dimensional derivative vector with respect to the parameters, calculated either analytically from equation (13) for Band fit or numerically for Band+PL fit. Note that a significant model uncertainty on $\Gamma_{\rm min}$ can arise if the photon with observed energy $E_{\rm max}$ is a random fluctuation of the underlying true spectrum that corresponds to $\Gamma \lesssim \Gamma_{\rm min}$ and $\tau_{\gamma\gamma}(E_{\rm max}) \gtrsim 1$. Also, the constraint on Γ as calculated here is relaxed if high-energy photons are produced throughout the "shell" rather than from the inner edge of the "shell" as assumed (or if the time dependence of the photon field is accounted for[SI33]).

Interval (s)	Spectrum	t_v (ms)	$\Gamma_{\rm min}$
0.6 – 0.8	Band+PL	14	951 ± 38
0.6 – 0.8	Band+PL	7	1043 ± 42
0.8 – 0.9	Band+PL	11.9	1218 ± 61
0.8 – 0.9	Band+PL	6	1357 ± 62
0.8 – 0.9	Band	11.9	1324 ± 50
0.8 – 0.9	Band	6	1493 ± 55

Table 3. $\Gamma_{\rm min}$ values for t_v = FWHM and FWHM/2

We estimate the variability time scale defined as a modified version of the rapidity index described in [SI34] We derive a differential of the light curve summed over all 4 bright NaI detectors (or 2 BGO detectors) at a given time resolution, ranging from 0.2 ms/bin to 200 ms/bin, at different time intervals during the GRB. The total variance per bin was then computed (a) within a GRB time interval and a narrow RoI centered on the GRB, as well as (b) well outside the GRB over the background region. The ratio of the two variances (a)/(b) is used as the variability index which is computed for various time resolutions. The time resolution at which the variability index peaks is defined as the intrinsic variability time scale of γ-ray emission in a particular time interval. This is similar to a method used more recently in [SI35] to estimate the variability time scale in terrestrial γ-ray flashes.

Table 2 shows the variability time scale estimated using the above method in time intervals $T_0 + 0.6$ s to $T_0 + 0.8$ s and $T_0 + 0.8$ s to $T_0 + 0.9$ s, and for both the NaI and the BGO detectors. We have also reported the full width at half maximum (FWHM) of the pulses in NaI and BGO detectors in these two time intervals.

As shown in Table 2 of the main text, a Band+PL spectral model is preferred in the $T_0 + 0.6$ s to $T_0 + 0.8$ s time interval while either Band or Band+PL spectral model fit the data well at $T_0 + 0.8$ s to $T_0 + 0.9$ s. Figure 8 shows our calculated $\Gamma_{\rm min}(t_v)$ for a Band+PL spectrum at 0.6 s – 0.8 s (*left panel*), and both the Band and Band+PL spectra at 0.8 s – 0.9 s (*right panel*). We choose to base the $\Gamma_{\rm min}$ calculation on the rise or decay times of the pulses, the sum of which is the FWHM, and therefore their average is t_v = FWHM/2. In the main text we conservatively quote the values of $\Gamma_{\rm min}$ for t_v = FWHM, but here we also provide its values for t_v = FWHM/2 (Table 3).

(6) Limits on Lorentz Invariance Violation or the Quantum Gravity Mass $M_{\rm QG}$

A. Limits on a possible time delay and on $M_{\rm QG}$

Some quantum-gravity (QG) theories allow violation of Lorentz invariance, and accordingly are consistent with dispersion in photon propagation: the photon speed $v_{\rm ph}$ may have a slight dependence on its energy, $E_{\rm ph}$, and the effect is expected to increase with $E_{\rm ph}$.[SI36] The high-energy photons can in principle travel either slower (sub-luminal: $v_{\rm ph} < c$) † or faster (super-luminal: $v_{\rm ph} > c$) than low-energy photons and thus arrive later (positive time delay) or earlier (negative time delay), respectively. We concentrate here mainly on positive time delays (the sub-luminal case) and only more briefly address negative time delays (the super-luminal case) near the end of this subsection, as they are somewhat harder to constrain using our data.

The Lorentz invariance violating (LIV) terms in the dependence of the photon momentum $p_{\rm ph}$ on the photon energy $E_{\rm ph}$ can be expressed as a power series,

$$\frac{p_{\rm ph}^2 c^2}{E_{\rm ph}^2} - 1 = \sum_{k=1}^{\infty} s_k \left(\frac{E_{\rm ph}}{\xi_k M_{\rm Planck} c^2} \right)^k = \sum_{k=1}^{\infty} s_k \left(\frac{E_{\rm ph}}{M_{{\rm QG},k} c^2} \right)^k \ , \tag{14}$$

in the ratio of $E_{\rm ph}$ and a typical energy scale $M_{{\rm QG},k}c^2 = \xi_k M_{\rm Planck} c^2$ for the $k^{\rm th}$ order, which is expected to be up to the order of the Planck scale, $M_{\rm Planck} = (\hbar c/G)^{1/2} \approx 1.22 \times 10^{19}$ GeV/c^2, where $s_k \in \{-1,\, 0,\, 1\}$. That is, $\xi_k = M_{{\rm QG},k}/M_{\rm Planck} \lesssim 1$ may naively be expected if $s_k \neq 0$ (i.e. in the terms that actually contribute to the sum). Since we observe photons of energy well below the Planck scale ($E_{\rm ph}/c^2 \ll M_{{\rm QG},k} \lesssim M_{\rm Planck}$), the dominant LIV term is associated with the lowest order non-zero term in the sum, of order $n = \min\{k | s_k \neq 0\}$, which is usually assumed to be either linear ($n = 1$) or quadratic ($n = 2$). The photon propagation speed is given by the corresponding group velocity,

$$v_{\rm ph} = \frac{\partial E_{\rm ph}}{\partial p_{\rm ph}} \approx c \left[1 - s_n \frac{n+1}{2} \left(\frac{E_{\rm ph}}{M_{{\rm QG},n} c^2} \right)^n \right] \ . \tag{15}$$

Note that $s_n = 1$ corresponds to the sub-luminal case (positive time delay), while $s_n = -1$ corresponds to the super-luminal case (negative time delay). Taking into account cosmological effects, this induces a time delay (or lag) in the arrival of a high-energy photon of energy $E_{\rm h}$, compared to a low-energy photon of energy $E_{\rm l}$ (emitted simultaneously at the same location), of[SI37]

$$\Delta t = s_n \frac{(1+n)}{2H_0} \frac{(E_h^n - E_l^n)}{(M_{{\rm QG},n} c^2)^n} \int_0^z \frac{(1+z')^n}{\sqrt{\Omega_m (1+z')^3 + \Omega_\Lambda}} \, dz' \ . \tag{16}$$

†Here, and throughout this work, $c \equiv \lim_{E_{\rm ph} \to 0} v_{\rm ph}(E_{\rm ph})$.

We adopt a standard $\Omega_M = 0.27$, $\Omega_\Lambda = 0.73$, $h = 0.71$ cosmology, throughout this work. For the redshift (z) and the energy of the high-energy photon (E_h) we conservatively use the value at the low end of the 1 σ confidence interval, i.e. we use $z = 0.900$ given the measured value of $z = 0.903 \pm 0.003$ and $E_h = 28.0$ GeV for the highest energy photon observed in GRB 090510 (which is the most constraining for LIV) given its measured energy of $E_h = 30.53^{+5.79}_{-2.56}$ GeV.

The low-energy ($\lesssim$ 1 MeV) prompt GRB light curve consists of many spikes, and it is sometimes hard to determine with much confidence from which of these spikes a particular high-energy photon was emitted. Moreover, individual spikes in GRB light curves sometimes show intrinsic lags in soft gamma rays (sub-MeV energies). In GRBs of the long-soft class such lags are usually manifested by the peak of the spike occurring earlier for higher energy photons, while for GRBs of the short-hard class there are either no measured lags or very short lags with equal probability for either sign. Such intrinsic lags have never been measured at much higher energies, but may also be present there (though they may exhibit somewhat different properties at such high energies) and it might be hard to disentangle intrinsic lags from a possible time delay induced by QG effects. Nevertheless, such intrinsic lags are thus far seen only on timescales of up to the width of individual spikes in a lightcurve, which for GRB 090510 are typically between a few milliseconds and a few tens of milliseconds.

If indeed a high-energy photon suffers a significant LIV induced time delay relative to low energy photons that are emitted simultaneously, then deriving its exact emission time is not straightforward. Therefore, to constrain $M_{\rm QG}$ we need to make some reasonable and conservative assumption about its emission time, given the fact that it is almost certainly physically associated with this short GRB. In the following we describe several possible different assumptions along with the astrophysical reasoning behind them and the corresponding lower limits that they imply on $M_{\rm QG}$ for the sub-luminal case ($s_n = 1$). We start from the most conservative assumption, and end with the least conservative assumption (which is nonetheless quite likely, and with good astrophysical motivation).

To derive most of our limits (for the sub-luminal case: $s_n = 1$) we do not attempt to associate the relevant high-energy photon with a particular spike in the low energy (soft gamma-ray) light curve. Instead, we simply assume that it was emitted sometime during the relevant emission episode, i.e. after its starting time $t_{\rm start}$ (while the start of such an emission episode is often marked by the onset of a particular spike, in most cases it includes additional spikes, and we allow the emission time of the high-energy photon to

be anytime during the relevant emission episode, regardless of the light curve structure during this time). This implies an upper limit on a possible LIV induced (positive) time lag, of $\Delta t < t_h - t_{\rm start}$ where t_h is the observed arrival time of the high-energy photon, and sets a lower limit on $M_{\rm QG,n}$ (for $s_n = 1$), that is proportional to its $E_h/\Delta t$ or $E_h/\Delta t^{1/2}$ for a linear or quadratic LIV, respectively (or $E_h/\Delta t^{1/n}$ in general). In GRB 090510 usually both $E_h/\Delta t$ and $E_h/\Delta t^{1/2}$ are largest for the 31 GeV photon (see the *solid* and *dashed* curves in panel (a) of main-text Fig. 1). Even when another photon gives higher values, we still conservatively use the values corresponding to the 31 GeV photon (which was observed at $t_h = T_0 + 0.829$ s, where T_0 is the GRB trigger time), as these are more robust and less sensitive to the exact choice of $t_{\rm start}$ or to intrinsic lags on the order of the width of individual spikes in the soft gamma-ray light curve.

We consider different possible assumptions about the emission time of the 31 GeV photon, namely different possible choices for $t_{\rm start}$, and calculate the corresponding limit on LIV, or more specifically the lower limits on $M_{\rm QG,1}$ and $M_{\rm QG,2}$ (or ξ_1 and ξ_2). Our four possible choices for $t_{\rm start}$ are shown by the vertical *dashed-dotted* lines in main-text Fig. 1.

The most conservative assumption would be to assume that the 31 GeV photon could have been emitted any time after the onset of the soft gamma-ray emission: $t_{\rm start} \approx T_0 - 30$ ms, corresponding to $\Delta t < 0.86$ s. Since the observed width of the relevant emission spike was at most a few tens of milliseconds, an intrinsic lag of that order would not have a significant effect on our results here. This most conservative limit already implies $\xi_1 > 1.19$ (i.e. $M_{\rm QG,1} > 1.19\, M_{\rm Planck}$).

However, it is highly unlikely that the 31 GeV photon is indeed associated with the small initial spike in the soft gamma-ray light curve that caused the GRB trigger, and it is much more likely associated with the main soft gamma-ray emission epoch that started at about $t_{\rm start} = T_0 + 0.53$ s. Moreover, it seems to be part of a distinct high-energy spectral component that develops only during this later main emission episode. This choice of $t_{\rm start}$, which is still quite conservative, corresponds to $\Delta t < 0.30$ s and $\xi_1 > 3.42$. The corresponding limits for $n = 1$ and $n = 2$ are:

$$M_{\rm QG,1} > 4.16 \times 10^{19} \left(\frac{E_{\rm h}}{28.0\ {\rm GeV}}\right) \left(\frac{\Delta t}{0.30\ {\rm s}}\right)^{-1} {\rm GeV/c^2}\ , \quad (17)$$

$$M_{\rm QG,2} > 5.05 \times 10^{10} \left(\frac{E_{\rm h}}{28.0\ {\rm GeV}}\right) \left(\frac{\Delta t}{0.30\ {\rm s}}\right)^{-1/2} {\rm GeV/c^2}\ , \quad (18)$$

where for the scaling with the photon energy we have used the approximation $E_h^n - E_l^n \approx E_h^n$ in eq. (16) because the high-energy (usually > 1 GeV) photons are much more energetic

than the low-energy (usually < 1 MeV) photons. The accurate expression is used to evaluate the numerical coefficient, and for calculating all of the numbers in Table 4 (even though the difference from the approximate values, which correspond to $E_l = 0$, is very small).

Moreover, for any reasonable emission spectrum, the emission of the 31 GeV photon would be accompanied by the emission of a large number of lower energy photons, which would suffer a much smaller time delay due to LIV effects, and would therefore mark its emission time. We could easily detect such photons in energies above 100 MeV, and therefore the fact that significant high-energy emission is observed only at later times (see main-text Fig. 1) strongly argues that the 31 GeV photon was not emitted before the onset of the observed high-energy emission. One could choose either the onset time of the emission above 100 MeV, which corresponds to $t_{\rm start} = T_0 + 0.648$ s, $\Delta t < 0.181$ s and $\xi_1 > 5.63$, or above 1 GeV, which corresponds to $t_{\rm start} = T_0 + 0.730$ s, $\Delta t < 99$ ms and $\xi_1 > 10.0$. We note that there is no evidence for the LIV induced energy dispersion that might be expected if indeed the 31 GeV photon was emitted near the above choices for $t_{\rm start}$, and was emitted together with lower energy photons, as can be expected for any reasonable emission spectrum. This is evident from the lack of accumulation of photons along the *solid* or *dashed* curves in panel (a) of main-text Fig. 1, and provides support for these choices of $t_{\rm start}$ (i.e. that they can indeed serve as upper limits for a possible LIV energy dispersion).

Finally, we note that the 31 GeV photon arrives near the peak of a very bright and narrow spike in the soft gamma-ray light curve, which has a width of $\sim 10 - 20$ ms, and if it is indeed associated with that spike then $|\Delta t| < 10$ ms (corresponding to the thin vertical shaded region in main-text Fig. 1) would imply $\xi_1 > 102$.

Moreover, this would imply a similar limit also on a **negative** time delay or lag of high-energy photons relative to low-energy photons (i.e. the super-luminal case: $s_n = -1$). This is in contrast to the previous limits that assumed emission after some starting time $t_{\rm start}$ but without an upper bound on the emission time, that can constrain only a positive time delay (corresponding to sub-luminal case: $s_n = 1$). For the super-luminal case ($s_n = -1$), we assume that the high-energy photon was emitted before the end of the low-energy spike, $t_{\rm end}$, i.e. $0 > \Delta t > t_h - t_{\rm end}$ or $-\Delta t = |\Delta t| < t_{\rm end} - t_h$. In our case the 31 GeV photon arrives approximately at the middle of the spike, $t_{\rm end} - t_h \approx t_h - t_{\rm start} \approx 10$ ms, resulting in a similar lower limit (of $\xi_1 > 102$) for the super-luminal ($s_1 = -1$) and sub-luminal ($s_1 = 1$) cases.

$t_{\rm start} - T_0$ (in ms)	limit on $\lvert\Delta t\rvert$ (ms)	Reason for choice of $t_{\rm start}$ or limit on Δt	E_l (MeV)	valid for s_n	lower limit on $M_{\rm QG,1}$ (10^{19} GeV/c^2)	($M_{\rm Planck}$)	limit on $M_{\rm QG,2}$ in 10^{10} GeV/c^2
-30	< 859	start of any < 1 MeV emission	0.1	1	> 1.45	$> \mathbf{1.19}$	> 2.99
530	< 299	start of main < 1 MeV emission	0.1	1	> 4.17	$> \mathbf{3.42}$	> 5.06
648	< 181	start of > 100 MeV emission	100	1	> 6.87	$> \mathbf{5.63}$	> 6.50
730	< 99	start of > 1 GeV emission	1000	1	> 12.2	$> \mathbf{10.0}$	> 8.79
—	< 10	association with < 1 MeV spike	0.1	± 1	> 125	$> \mathbf{102}$	> 27.7
—	< 19	if 0.75 GeV γ is from $1^{\rm st}$ spike	0.1	-1	> 1.76	$> \mathbf{1.33}$	> 0.54
$\lvert\Delta t/\Delta E\rvert < 30$ ms/GeV		lag analysis of > 1 GeV spikes	—	± 1	> 1.49	$> \mathbf{1.22}$	—

Table 4. Lower limits on the Quantum Gravity (QG) mass scale associated with possible Lorentz Invariance Violation (LIV), that we can place from the lack of time delay in the arrival of high-energy photons relative to low energy photons, from our observations of GRB 090510.

A weaker but independent and somewhat more robust limit on a possible **negative** time delay or lag (which constrains the super-luminal case, $s_n = -1$) may be obtained from the ≈ 750 MeV photon that is observed during the first soft gamma-ray spike near the trigger time. This photon has a high probability of being from GRB 090510 (a chance probability of $\sim 1.2 \times 10^{-6}$ corresponding to $\sim 4.6\ \sigma$), and the 1-σ confidence interval for its energy is 693.6 – 854.4 MeV. The associated maximum time delay $\Delta t < 19$ ms for that photon implies $\xi_1 > 1.33$, when conservatively using the 1-σ lower limit on its energy.

Finally, we obtain a limit of $\lvert\Delta t/\Delta E\rvert < 30$ ms/GeV (at 99% confidence) on a linear energy dispersion ($n = 1$) through a lag analysis of the high-energy photons, as described in subsection 1-B-2. Our limits are summarized in Table 4.

Our limits are the most stringent constraints to date. The previous best lower limits from GRBs[SI19] are 1.3×10^{18} GeV (linear) and 8.2×10^9 GeV (quadratic) based on a similar line of reasoning for the LAT GRB 080916C. For active galaxies, spectral lags during a TeV flare from Markarian 501 reported by the MAGIC collaboration[SI38] indicate $M_{\rm QG,1} > 2.1 \times 10^{17}$ GeV/c^2 and $M_{\rm QG,2} > 2.6 \times 10^{10}$ GeV/c^2 at 95% confidence level.

B. Implications of the limit on $M_{\rm QG}$

Various quantum gravity scenarios postulate that physics can be strongly modified owing to the possible inherent structure of space-time on the Planck scale, $\lambda_{\rm Planck} = (G\hbar/c^3)^{1/2} \approx 1.62 \times 10^{-33}$ cm. It has been proposed that Lorentz invariance violation (LIV) may occur at high energy associated with the quantum gravity mass scale $M_{\rm QG}$, usually assumed to be close to $M_{\rm Planck}$. This could have various astrophysical consequences that might be manifested in a suppressed form at an energy scale $\ll M_{\rm QG}c^2$.

Among other testable potential astrophysical phenomena predicted is a possible variation of the photon propagation speed with its energy $E_{\rm ph}$.[SI36] A specific model of particular interest that has been proposed is a space-time foam scenario inspired by string theory that predicts a small retardation of photon velocity to first order in $E_{\rm ph}/M_{\rm QG}$,[SI39] which is equivalent to a vacuum index of refraction $1+(E_{\rm ph}/M_{\rm QG})$. This results in a time delay Δt between the arrival times of two photons of energies $E_h > E_l$ that is given by eq. (16). Here we consider mainly theories in which the leading LIV term is linear in $E_{\rm ph}/M_{\rm QG}$ (i.e. $n = 1$), for which eq. (16) simplifies to

$$\Delta t = \frac{\Delta E}{H_0 M_{{\rm QG},n} c^2} \int_0^z \frac{(1+z')}{\sqrt{\Omega_m (1+z')^3 + \Omega_\Lambda}}\, dz' \ , \tag{19}$$

where $\Delta E = E_h - E_l$. This expression has already been used in conjunction with *Fermi* observations of GRB080916C to give the constraint of $M_{\rm QG,1} \gtrsim 0.1 M_{\rm Planck}$.[SI19]

Here we use the new observations of GRB 090510 to derive the constraint $M_{\rm QG,1}/M_{\rm Planck} \gtrsim$ several (or even $\gtrsim 100$ for our least conservative limit). This is a more fundamentally meaningful constraint. Since, in the space-time foam scenario, $M_{\rm QG} \lesssim M_{\rm Planck}$, our new constraints make this model highly implausible. Our results do not significantly constrain any theoretical models that suppress $n = 1$ terms and are characterized by $n \geq 2$ terms. For example, in effective field theory models with Planck scale modifying dimension-six operators, $n = 1$ terms arising from lower dimension operators can be suppressed by a symmetry such as CPT conservation.[SI40]

Another quantum gravity model that explores the addition of a logarithmic correction to the quantum mechanical wave equation of a particle has also been found[SI41] to give a vacuum dispersion relation where the photon velocity is modified by a term that approximates an expression that is linear in $E_{\rm ph}/M_{\rm QG}$, as in the model of .[SI39] This model also is strongly disfavored by our analysis of GRB 090510.

It has been shown that the constraints on first order energy dependent fractional time delays of the order of $\Delta t/t \sim E_{\rm ph}/M_{\rm Planck}$ (where t is the total flight time from the source to us, and Δt is relative to a much lower energy photon $E_l \ll E_h = E_{\rm ph}$ emitted simultaneously) can be related to the predicted absorption of gamma-rays with energies above $\sim$ 10 TeV by interactions with the extragalactic background light.[SI42] This is due the increase in the threshold energy for the annihilation of gamma rays into electron-positron pairs, owing to LIV, which would make the universe more transparent to gamma rays than expected without LIV.[SI43,SI44] An analysis of the multi-TeV gamma-ray spectrum from Mkn 501 has been used[SI45] to put constraints on Lorentz invariance

violation of the order of $\lesssim 10^{-15}$. This result was then used[SI46] to place a lower limit on the quantum gravity mass of $M_{\mathrm{QG},1} \gtrsim 0.3 M_{\mathrm{Planck}}$ with the constraint given by $M_{\mathrm{QG},1} \geq E^3_{\mathrm{max}}/8m_e^2c^6$ if there is no indication of gamma-ray absorption up to a photon energy of E_{max}. Our results predict an unmodified absorption in extragalactic gamma-ray spectra at energies above ~ 20 TeV.

SI1. Abdo, A. A., et al. "Fermi observations of high-energy gamma-ray emission from GRB 080825C", *Astrophys. J., submitted* (2009).

SI2. W. B. Atwood et al, "The Large Area Telescop on the Fermi gamma-ray space telescope mission", *Atrophys. J.*, **697**, 1071–1102 (2009).

SI3. T. M. Koshut et al., "Systematic Effects on Duration Measurements of Gamma-Ray Bursts", *Astrophys. J.*, **463**, 570–592 (1996).

SI4. Norris, J. P., & Bonnell, J. T. " Short Gamma-Ray Bursts with Extended Emission, *Astrophys. J.*, **643**, 266–275 (2006).

SI5. J. D. Scargle, J. P. Norris & J. T. Bonnell, "An Algorithm for Detecting Quantum Gravity Photon Dispersion in Gamma-Ray Bursts: DisCan", *Astrophys. J.*, **673**, 972–980 (2008).

SI6. M. S. Bartlett, "Stochastic Processes", Cambridge University Press (1978).

SI7. G. Ghisellini, L. Maraschi, & L. Dondi, "Diagnostics of Inverse-Compton models for the gamma-ray emission of 3C 279 and MKN 421", *Astronomy and Astrophysics Supplements*, **120**, 503–506 (1996).

SI8. Waxman, E. "Cosmological Gamma-Ray Bursts and the Highest Energy Cosmic Rays", *Phys. Rev. Lett.*, **75**, 386–389 (1995).

SI9. Vietri, M. "The Acceleration of Ultra–High-Energy Cosmic Rays in Gamma-Ray Bursts, *Astrophys. J.*, 453, 883–886 (1995).

SI10. Vietri, M. "GeV Photons from Ultrahigh Energy Cosmic Rays Accelerated in Gamma Ray Bursts", *Phys. Rev. Lett.*, **78**, 4328–4331 (1997).

SI11. Rachen, J. P., & Mészáros, P. "Photohadronic neutrinos from transients in astrophysical sources", *Phys. Rev. D*, **58**, 123005–123018 (1998).

SI12. Böttcher, M., & Dermer, C. D. "High-energy Gamma Rays from Ultra-high-energy Cosmic-Ray Protons in Gamma-Ray Bursts", *Astrophys. J.*, **499**, L131–L134 (1998).

SI13. Dermer, C. D. "Neutrino, Neutron, and Cosmic-Ray Production in the External Shock Model of Gamma-Ray Bursts", *Astrophys. J.*, **574**, 65–87 (2002).

SI14. Dermer, C. D., & Atoyan, A. "Ultra-high energy cosmic rays, cascade gamma rays, and high-energy neutrinos from gamma-ray bursts," *New J. of Phys.*, **8**, 122–136 (2006).

SI15. Gupta, N., & Zhang, B. "Prompt emission of high-energy photons from gamma ray bursts", *Mon. Not. Roy. Ast. Soc.*, **380**, 78–92 (2007).

SI16. Coppi, P. S. "Time-dependent models of magnetized pair plasmas", **258**, 657–683 (1992).

SI17. Asano, K., Inoue, S., & Mészáros, P. "Prompt High-Energy Emission from Proton-Dominated Gamma-Ray Bursts", *Astrophys. J.*, **699**, 953–957 (2009).

SI18. Asano, K., Guiriec, S., & Mészáros, P. in preparation (2009)

SI19. Abdo, A. A., et al. Fermi Observations of High-Energy Gamma-Ray Emission from GRB 080916C. *Science*, **323**, 1688–1693 (2009).

SI20. S. Razzaque, C.D. Dermer, & J. Finke, "Synchrotron radiation from ultra-high energy protons and the Fermi observations of GRB 080916C". *Astrophys. J. Lett.*, submitted (2009).

SI21. K. Murase, "Prompt high-energy neutrinos from gamma-ray bursts in photospheric and synchrotron self-Compton scenarios", *Phys. Rev. D*, **78**, 101302–1013xx (2008).

SI22. Hauser, M. G., & Dwek, E. "The Cosmic Infrared Background: Measurements and Implications," *Annual Reviews Astron. Astrophys.*, **39**, 249–307 (2001).

SI23. Stecker, F. W., Malkan, M. A., & Scully, S. T. "Intergalactic Photon Spectra from the Far-IR to the UV Lyman Limit for 0 ¡ z ¡ 6 and the Optical Depth of the Universe to High-Energy Gamma Rays", *Astrophys. J.*, **648**, 774–783 (2006).

SI24. Gilmore, R. C., Madau, P., Primack, J. R., Somerville, R. S., & Haardt, F. "GeV Gamma-Ray Attenuation and the High-Redshift UV Background", *Mon. Not. Roy. Ast. Soc.*, submitted, arXiv:0905.1144 (2009).

SI25. Kneiske, T. M., Bretz, T., Mannheim, K., & Hartmann, D. H. "Implications of cosmological gamma-ray absorption. II. Modification of gamma-ray spectra", *Astron. Astrophys.*, **413**, 807–815 (2004).

SI26. Franceschini, A., Rodighiero, G., & Vaccari, M. "Extragalactic optical-infrared background radiation, its time evolution and the cosmic photon-photon opacity", *Astron. Astrophys.*, **487**, 837–852 (2008).

SI27. Finke, J. D., Razzaque, S., & Dermer, C. D. "Modeling the Extragalactic Background Light from Stars and Dust", *Astrophys. J.*, submitted, arXiv:0905.1115 (2009).

SI28. Greiner, J., *et al.* The redshift and afterglow of the extremely energetic gamma-ray burst GRB 080916C. submitted to *Astron. Astrophys.* (arXiv:0902.0761) (2009).

SI29. Lithwick. Y. & Sari, R. Lower Limits on Lorentz Factors in Gamma-Ray Bursts. *Astrophys. J.*, **555**, 540–545 (2001).

SI30. Razzaque, S., Mészáros, P., & Zhang, B. GeV and Higher Energy Photon Interactions in Gamma-Ray Burst Fireballs and Surroundings. *Astrophys. J.*, **613**, 1072–1078 (2004).

SI31. Gould, R. J., & Schréder, G. P. Opacity of the Universe to High-Energy Photons. *Phys. Rev.*, **155**, 1408–1411 (1967).

SI32. Brown, R. W., Mikaelian, K. O., & Gould, R. J. Absorption of High-Energy Cosmic Photons through Double-Pair Production in Photon-Photon Collisions. *Astrophys. Lett.*, **14**, 203 (1973).

SI33. Granot, J., Cohen-Tanugi, J. & do Couto e Silva, E. Opacity Buildup in Impulsive Relativistic Sources. *Astrophys. J.*, **677**, 92–126 (2008).

SI34. Bhat, P. N., Fishman, G. J., Meegan, C. A., Wilson, R. B., & Paciesas, W. S., *AIP Conf. Proc.*, **307**, 197 (1993)

SI35. Nemiroff, J., Bonnell, J. T., & Norris, J. P., *J. of Geophysical Res.*, **102**, 9659 (1997).

SI36. Amelino-Camelia, G., Ellis, J., Mavromatos, N. E., Nanopoulos, D. V., Sarkar, S. "Tests of quantum gravity from observations of gamma-ray bursts", *Nature*, **393**, 763–765 (1998).

SI37. Jacob, U., & Piran, T. "Lorentz-violation-induced arrival delays of cosmological particles", *J. Cosmol. Astropart. Phys.*, **01**, 031 (2008).

SI38. Albert, J. et al. "Probing quantum gravity using photons from a flare of the active galactic nucleus Markarian 501 observed by the MAGIC telescope", *Phys. Lett. B*, **668**, 253–257 (2008).

SI39. Ellis, J., Mavromatos, N. E., & Nanopoulos, D. V. "Derivation of a vacuum refractive index in a stringy space time foam model", *Phys. Lett. B* **665**, 412–417 (2008), and references therein.

SI40. Bolokhov, P. A., Nibbelink, S. G. & Pospelov, M. "Lorentz Violating Supersymmetric Quantum Electrodynamics", *Phys. Rev. D*, **72**, 015013-1 – 015013-17 (2005).

SI41. Zloshchstiev, K. G., arXiv:0906.4282 [hep-th].

SI42. Kifune, T. "Invariance Violation Extends the Cosmic-Ray Horizon? " *Astrophys. J.*, **518**, L21–L24 (1999).

SI43. Coleman, S. & Glashow, S. L. "High-energy tests of Lorentz invariance", *Phys. Rev. D*, **59**, 116008 (1999).

SI44. Jacob, U., & Piran, T. "Inspecting absorption in the spectra of extra-galactic gamma-ray sources for insight into Lorentz invariance violation", *Phys. Rev. D*, **78**, 124010 (2008).

SI45. Stecker, F. W. & Glashow, S. L. "New tests of Lorentz invariance following from observations of the highest energy cosmic γ-rays", *Astropart. Phys.*, **16**, 97–99 (2001).

SI46. Stecker, F. W. "Constraints on Lorentz invariance violating quantum gravity and large extra dimensions models using high energy γ-ray observations", *Astropart. Phys.*, **20**, 85–90 (2003).